Theoretical Investigation of One-Photon and Two-Photon Absorption Properties for Multiply N-Confused Porphyrins

Zhao-Di Yang,[†,‡] Ji-Kang Feng,*[,†,§] Ai-Min Ren,[†] and Chia-Chung Sun[†]

State Key Laboratory of Theoretical and Computational Chemistry, Jilin University, Changchun 130023, China, The College of Chemistry, Jilin University, Changchun 130023, China, and Chemical and Environmental Engineering College, Harbin University of Science and Technology, Harbin 150080, China

Received: July 7, 2006; In Final Form: October 12, 2006

We have theoretically investigated a series of multiply N-confused porphyrins and their Zn or Cu complexes for the first time by using DFT(B3LYP/6-31G*) and ZINDO/SOS methods. The electronic structure, one-photon absorption (OPA), and two-photon absorption (TPA) properties have been studied in detail. The calculated results indicate that the OPA spectra of multiply N-confused porphyrins are red-shifted and the OPA intensities decrease compared to normal porphyrin. The maximum two photon absorption wavelengths λ_{max} are blue-shifted and the TPA cross sections δ_{max} are increased 22.7−112.1 GM when the N atoms one by one are inverted from core to β position to form multiply N-confused porphyrins. Especially δ_{max} of N_3CP get to 164.7 GM. The electron donors $-C_6F_5$s at meso-position can make the TPA cross section δ_{max} increase. After forming metal complexes with Cu or Zn, the TPA properties of multiply N-confused porphyrins are further increased except for N_3CP, N_4CP. Our theoretical findings demonstrate that the multiply N-confused prophyrins as well as their metal complexes and derivatives are promising molecules that can be assembled series of materials with large TPA cross section, and are sure to be the subject of further investigation.

Introduction

Porphyrin is a well-known tetrapyrrolic macrocycle that has four nitrogen atoms arranged inside the core that are able to coordinate a variety of metal ions. Normally, the porphyrin core is considered to be planar because of the resonance stabilization resulting from the 18-π electron aromatic system.[1,2] By contrast, its N-confused analogues display versatile structures. Maeda et al.[3,4] first synthesized a novel porphyrin isomer (N_1CP) in which one of the four pyrrole rings is connected at α and β positions to meso carbons. These N-confused porphyrins can chelate metal cations in the core to give square-planar complexes like normal prophyrin. Later they synthesized further "evolved" confused isomers: multiply N-confused porphyrins with two or more confused pyrrole rings as showed in Figure 1.[5−7] Since the casual discovery of N-confused porphyrin a number of unusual properties that are different from normal porphyrins have been disclosed in a variety of confused porphyrinoids.[8−10] However, few theoretical studies focus on the photochemical properties of these multiply N-confused porphyrins, especially for the TPA property.

The study of TPA properties of porphyrins has been the focus of many recent works because they are suitable candidates for a number of possible applications, such as building optical limiting devices, requiring a high TPA absorption cross section.[11,12] Furthermore, they can be of interest for the pharmaceutical industry, since their pronounced TPA in the infrared region can be exploited in the field of photodynamic therapy.[13] It is well-known that the TPA cross section value of porphyrin itself is small (a few tens GM),[14,15] but we can design and synthesize all kinds of its derivatives to increase the conjugation property. Now many porphyrin derivatives and analogues have been designed and synthesized, at the same time they were found possessing a large TPA cross section.[16−19] On second thought, the N-confused porphyrins analogues should have similar or better photochemical properties compared to normal porphyrin. Thus in this work, in order to provide some useful information on designing and synthesizing new materials with large TPA cross section values, the equilibrium geometries, the electronic structures, and OPA and TPA properties of multiply N-confused porphyrins and their corresponding metal complexes have been

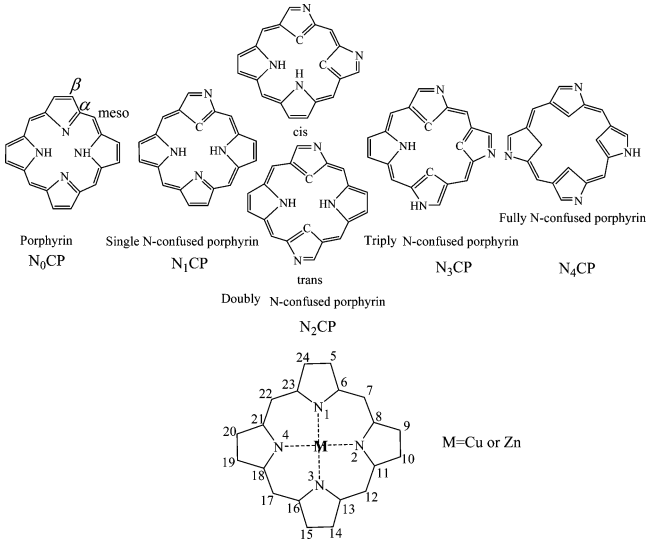

Figure 1. The investigated molecules and corresponding names and labels.

* Corresponding author. E-mail: JiKangf@yahoo.com. Fax: (+86)431-8945942.

† State Key Laboratory of Theoretical and Computational Chemistry, Jilin University.

‡ Harbin University of Science and Technology.

§ The College of Chemistry, Jilin University.

10.1021/jp0642802 CCC: $33.50
Published on Web 12/07/2006

investigated compared to normal porphyrin. The structure−property relationship has been revealed.

Computational Methods

The TPA process corresponds to simultaneous absorption of two photons. The TPA efficiency of an organic molecule, at optical frequency $\omega/2\pi$, can be characterized by the TPA cross section $\delta(\omega)$. It can be directly related to the imaginary part of the third-order polarizability $\gamma(-\omega;\omega,\omega,-\omega)$[20,21] as showed in eq 1,

$$\delta(\omega) = \frac{3\hbar\omega^2}{2n^2c^2\epsilon_0} L^4 \,\mathrm{Im}\,\gamma(-\omega;\omega,\omega,-\omega) \qquad (1)$$

where $\gamma(-\omega;\omega,\omega,-\omega)$ is the third-order polarizability, $\hbar\omega$ is the energy of incoming photons, c is the speed of light, ϵ_0 is the vacuum electric permittivity, n denotes the refractive index of the medium, and L corresponds to the local-field factor. In the calculations presented here, n and L are set to 1 because of isolated molecule in vacuum.

The sum-over-states (SOS) expression to evaluate the components of the second hyperpolarizability $\gamma_{\alpha\beta\gamma\delta}$ can be educed out using perturbation theory. By considering a Taylor expansion of energy with respect to the applied field, the $\gamma_{\alpha\beta\gamma\delta}$ Cartesian components are given by refs 22 and 23.

$$\gamma_{\alpha\beta\gamma\delta}(-\omega_\sigma;\omega_1,\omega_2,\omega_3) = \hbar^{-3}\sum P_{1,2,3}$$

$$\Bigg(\sum_K{}' \sum_L{}' \sum_M{}' \times \Bigg(\frac{\langle 0|\mu_\alpha|K\rangle\langle K|\overline{\mu_\beta}|L\rangle\langle L|\overline{\mu_\gamma}|M\rangle\langle M|\mu_\delta|0\rangle}{(\omega_K - i\Gamma_K/2 - \omega_\sigma)(\omega_L - i\Gamma_L/2 - \omega_2 - \omega_3)(\omega_M - i\Gamma_M/2 - \omega_3)}$$

$$+ \frac{\langle 0|\mu_\beta|K\rangle\langle K|\overline{\mu_\alpha}|L\rangle\langle L|\overline{\mu_\gamma}|M\rangle\langle M|\mu_\delta|0\rangle}{(\omega_K + i\Gamma_K/2 + \omega_1)(\omega_L - i\Gamma_L/2 - \omega_2 - \omega_3)(\omega_M - i\Gamma_M/2 - \omega_3)}$$

$$+ \frac{\langle 0|\mu_\beta|K\rangle\langle K|\overline{\mu_\gamma}|L\rangle\langle L|\overline{\mu_\alpha}|M\rangle\langle M|\mu_\delta|0\rangle}{(\omega_K + i\Gamma_K/2 + \omega_1)(\omega_L + i\Gamma_L/2 + \omega_2 + \omega_3)(\omega_M - i\Gamma_M/2 - \omega_3)}$$

$$+ \frac{\langle 0|\mu_\beta|K\rangle\langle K|\overline{\mu_\gamma}|L\rangle\langle L|\overline{\mu_\delta}|M\rangle\langle M|\mu_\alpha|0\rangle}{(\omega_K + i\Gamma_K/2 + \omega_1)(\omega_L + i\Gamma_L/2 + \omega_2 + \omega_3)(\omega_M + i\Gamma_M/2 + \omega_3)}\Bigg)$$

$$- \sum_K{}' \sum_L{}' \times \Bigg(\frac{\langle 0|\mu_\alpha|K\rangle\langle K|\mu_\beta|0\rangle\langle 0|\mu_\gamma|L\rangle\langle L|\mu_\delta|0\rangle}{(\omega_K - i\Gamma_K/2 - \omega_\sigma)(\omega_K - i\Gamma_K/2 - \omega_1)(\omega_L - i\Gamma_L/2 - \omega_3)}$$

$$+ \frac{\langle 0|\mu_\alpha|K\rangle\langle K|\mu_\beta|0\rangle\langle 0|\mu_\gamma|L\rangle\langle L|\mu_\delta|0\rangle}{(\omega_K - i\Gamma_K/2 - \omega_1)(\omega_L + i\Gamma_L/2 + \omega_2)(\omega_L - i\Gamma_L/2 - \omega_3)}$$

$$+ \frac{\langle 0|\mu_\beta|K\rangle\langle K|\mu_\alpha|0\rangle\langle 0|\mu_\gamma|L\rangle\langle L|\mu_\delta|0\rangle}{(\omega_K + i\Gamma_K/2 + \omega_1)(\omega_K + i\Gamma_K/2 + \omega_o)(\omega_L + i\Gamma_L/2 + \omega_2)}$$

$$+ \frac{\langle 0|\mu_\beta|K\rangle\langle K|\mu_\alpha|0\rangle\langle 0|\mu_\gamma|L\rangle\langle L|\mu_\delta|0\rangle}{(\omega_K + i\Gamma_K/2 + \omega_1)(\omega_L + i\Gamma_L/2 + \omega_2)(\omega_L - i\Gamma_L/2 - \omega_3)}\Bigg)\Bigg) \qquad (2)$$

In the formula α, β, γ, and δ refer to the molecular axes; ω_1, ω_2, and ω_3 are optical frequencies, and $\omega_\sigma = \omega_1 + \omega_2 + \omega_3$ is the polarization response frequency; $\sum P_{1,2,3}$ indicates a sum over the terms obtained by the six permutations of the pairs (ω_1/μ_β), (ω_2/μ_γ), and (ω_3/μ_δ); K, L, and M denote excited states and 0 denotes the ground state; $|K\rangle$ is an electronic wavefunction with energy $\hbar\omega_K$ relative to the ground electronic state; μ_α is the αth$(= x, y, z)$ component of the dipole operator, $\langle K|\overline{\mu_\alpha}|L\rangle = \langle K|\mu_\alpha|L\rangle - \langle 0|\mu_\alpha|0\rangle\delta_{KL}$; the primes on the summation over the electronic states indicate exclusion of the ground state. Γ_K is the damping factor of excited state K, and in the present work, all damping factor are set to 0.14 eV; this choice of damping factor is found to be reasonable on the basis of the comparison between the theoretically calculated and experimental TPA spectra.[24,25] To compare the calculated δ value with the experimental value measured in solution, the orientationally averaged (isotropic) value of γ is evaluated, which is defined as

$$\langle\gamma\rangle = \frac{1}{15}\sum_{i,j}(\gamma_{iijj} + \gamma_{ijij} + \gamma_{ijji}) \qquad i, j = x, y, z \qquad (3)$$

When the imaginary part of the $\langle\gamma\rangle$ value is substituted into expression 1, $\delta(\omega)$ that can be compared with the experimental value is obtained.

In this paper, all the geometries of molecules are optimized by the B3LYP/6-31G(d) method. Then the properties of electronic excited states were obtained by single electron excitations and double electron excitation configuration interaction (SDCI) using the ZINDO program. Futhermore, the transition energies and transition dipole moment needed to predict the TPA cross section were also provided. Then, we compiled a program to calculate the second hyperpolarizability γ and the TPA cross section according to eqs 1 and 2.

Results and Discussions

1. Geometry Optimization and Electronic Structure. The investigated molecules are shown in Figure 1, including normal porphyrin (N_0CP), singly N-confused porphyrin (N_1CP), doubly N-confused porphyrin (*cis*-N_2CP or *trans*-N_2CP), triply N-confused porphyrin (N_3CP), fully N-confused porphyrin (N_4-CP), and their Cu or Zn complexes: N_0CPZn(II) (ZnP), N_1CPZn(II), N_2CPCu(III) N_3CPZn(IV), N_4CPZn(IV). In these five kinds of N-confused porphyrins, each kind of N-confused porphyrin has many tautomers.[26] We choose the lowest potential energy tautomer here, and the optimized results are identical with those in ref 26 by Furuta et al. using B3LYP/6-31G**. The geometry parameters are shown in Table 1. The optimized results show that there is D_{2h} symmetry for N_0CP, C_2 symmetry for *cis*-N_2CP, C_i symmetry for *trans*-N_2CP, D_{4h} symmetry for N_0CPZn (ZnP), and C_s symmetry for N_1CPZn(II), N_2CPCu-(III), N_3CPZn(IV), and N_4CPZn(IV). N_1CP, N_3CP, and N_4CP have no symmetry constraints. As shown in Table 1, the bond lengths of confused pyrrole rings in the multiply N-confused porphyrins change much (shown in boldface in Table 1) but the bond lengths of nonconfused pyrrole rings change little compared with normal prophyrin, and the planar structure was distorted owing to space potential block as a result of center N turning to center C after inverting N atom in pyrrole ring to β position. Consequently, the distances of center C or N change a little, about 0.0002−0.3 Å, and the dihedral angles have a large change. In the *trans*-N_2CP, the two confused pyrrole rings bent to the same side at 22.0° and 20.7°, and these values are close to the X-ray diffraction results 21.9° and 21.2°.[6] However, the relative position of four meso-C has little distortion and the dihedral angle only deviates 0.24−2.2° as shown in Table 1. All the metal complexes are rather planar, which is very much in accord with experiment,[6,9] and the bond lengths of metal complexes of multiply N-confused porphyrins are generally smaller than those of corresponding multiply N-confused porphyrins. The bond lengths of Cu−C and Cu−N in *cis*-N_2-

TABLE 1: Geometry Parameters of Studied Molecules (Å)[a]

	N_0CP (D_{2h})	N_1CP (C_1)	*cis*-N_2CP (C_2)	*trans*-N_2CP (C_i)	N_3CP (C_1)	N_4CP (C_1)
selected bonds						
r(1,3)	4.0600	4.0058	4.2376	3.9847	**4.1990**	**4.2648**
r(2,4)	4.2340	4.3800	4.2375	4.5341	**4.4218**	**4.1630**
r(5,24)	1.3565	**1.3026**	**1.3055**	**1.3021**	**1.3031**	**1.3045**
r(5,6)	1.4601	**1.4223**	**1.4193**	**1.4221**	**1.4190**	**1.4186**
r(6,7)	1.4001	1.3973	1.4033	1.4027	**1.3823**	**1.3724**
r(7,8)	1.3940	1.3992	1.4033	1.4011	**1.4317**	**1.4488**
r(8,9)	1.4349	1.4320	**1.4193**	1.4334	**1.4757**	**1.4036**
r(9,10)	1.3722	1.3769	**1.3055**	1.3782	**1.3046**	**1.3602**
r(10,11)	1.4349	1.4315	**1.4713**	1.4338	**1.4229**	**1.3971**
r(11,12)	1.3940	1.3983	1.4083	1.4000	**1.3765**	**1.4407**
r(12,13)	1.4001	1.4006	1.3935	1.4052	**1.4375**	**1.3729**
r(13,14)	1.4601	1.4599	1.4278	**1.4716**	**1.4017**	**1.4185**
r(14,15)	1.3565	1.3545	1.3765	**1.3021**	**1.3584**	**1.3044**
r(15,16,)	1.4601	1.4602	1.4318	**1.4221**	**1.4003**	**1.4823**
r(16,17)	1.4001	1.4033	1.4002	1.4027	**1.4333**	**1.4457**
r(17,18)	1.3940	1.3958	1.4002	1.4011	**1.3798**	**1.3670**
r(18,19)	1.4349	1.4342	1.4318	1.4334	**1.4494**	**1.3975**
r(19,20)	1.3722	1.3745	1.3765	1.3782	**1.3644**	**1.3143**
r(20,21)	1.4349	1.4347	1.4278	1.4338	**1.4476**	**1.4518**
r(21,22)	1.3940	1.3952	1.3935	1.4000	**1.3804**	**1.3671**
r(22,23)	1.4001	1.4030	1.4083	1.4052	**1.4285**	**1.4461**
r(23,24)	1.4601	**1.4711**	**1.4713**	**1.4716**	**1.4771**	**1.4796**
r(1,6)	1.3633	**1.4093**	**1.4099**	**1.4036**	**1.4354**	**1.4395**
r(1,23)	1.3633	**1.4046**	**1.4023**	**1.4106**	**1.3854**	**1.3796**
r(2,11)	1.3725	1.3799	**1.4099**	1.3758	**1.3824**	**1.4244**
r(2,8)	1.3725	1.3697	**1.4023**	1.3762	**1.4289**	**1.3878**
r(3,13)	1.3633	1.3720	1.3988	**1.4106**	**1.4324**	**1.4403**
r(3,16)	1.3633	1.3692	1.3849	**1.4136**	**1.3887**	**1.3790**
r(4,18)	1.3725	1.3698	1.3849	1.3758	**1.3852**	**1.5024**
r(4,21)	1.3725	1.3812	1.3988	1.3762	**1.3887**	**1.4979**
selected dihedral angles						
d(H,1,6,7)	0	17.8	14.5	20.7(21.2)		
d(H,3,16,17)	0		24.9	22.0(21.9)		
d(7,12,17,22)	0	0.60	0	0	−2.2	−0.24

	$N_0CPZn(II)$ (D_{4h})	$N_1CPZn(II)$ (C_s)	*cis*-$N_2CPCu(III)$ (C_s)	*trans*-$N_2CPCu(III)$ (C_s)	$N_3CPZn(IV)$ (C_s)	$N_4CPZn(IV)$ (C_s)
selected bonds						
r(1,Cu(Zn))		1.9523	1.9272(1.9393)	1.9228(1.9407)	1.9669	1.9885
r(2,Cu(Zn))		2.1346	1.9264(1.9344)	1.9751(1.9676)	2.0304	1.9894
r(3,Cu(Zn))		1.9886	1.9902(1.9693)	1.9369(1.9447)	1.9719	2.0009
r(4,Cu(Zn))		2.1310	1.9825(1.9544)	1.9745(1.9656)	1.9889	1.9984
r(5,24)		1.3450	1.2984	1.2948	1.3477	1.3015
r(5,6)		1.4192	1.4148	1.4311	1.4029	1.4267
r(6,7)		1.4115	1.3652	1.3709	1.4120	1.4325
r(7,8)		1.3915	1.4026	1.3957	1.3674	1.3641
r(8,9)		1.4519	1.3946	1.4375	1.4096	1.4657
r(9,10)		1.3639	1.3418	1.3569	1.3060	1.3013
r(10,11)		1.4536	1.4086	1.4380	1.4537	1.4287
r(11,12)		1.4090	1.4080	1.3695	1.4634	1.4377
r(12,13)		1.3920	1.3659	1.4037	1.3713	1.3614
r(13,14)		1.4539	1.4436	1.4084	1.4195	1.4134
r(14,15)		1.3566	1.3549	1.3422	1.2995	1.3020
r(15,16,)		1.4539	1.4471	1.4056	1.4709	1.4741
r(16,17)		1.3912	1.3868	1.3923	1.3914	1.4364
r(17,18)		1.4105	1.3827	1.3754	1.3848	1.3634
r(18,19)		1.4565	1.4451	1.4369	1.4418	1.4144
r(19,20)		1.3613	1.3567	1.3576	1.3591	1.3022
r(20,21)		1.4548	1.4414	1.4365	1.4425	1.4717
r(21,22)		1.3840	1.3749	1.3870	1.3776	1.4319
r(22,23)		1.4260	1.3939	1.3804	1.4007	1.3656
r(23,24)		1.4171	1.4658	1.4728	1.4042	1.4655
r(1,6)		1.3948	1.4347	1.4163	1.4251	1.3788
r(1,23)		1.4251	1.4043	1.4041	1.3987	1.4409
r(2,11)		1.3788	1.3994	1.3786	1.4378	1.3763
r(2,8)		1.3530	1.4333	1.4067	1.3998	1.4413
r(3,13)		1.3808	1.3949	1.4252	1.4182	1.4473
r(3,16)		1.3814	1.3712	1.3950	1.4061	1.3770
r(4,18)		1.3496	1.3777	1.3993	1.3830	1.4444
r(4,21)		1.3861	1.3857	1.3878	1.3912	1.3805

[a] The values in parentheses are the experimental observation of X-ray diffraction.

TABLE 2: The Calculated Frontier Orbital Energy Data (eV)

N_0CP	N_1CP	*cis*-N_2CP	*trans*-N_2CP	N_3CP	N_4CP
		Virtual Orbitals			
2.45	2.28	1.85	2.03	1.90	1.79
2.16	1.95	1.64	1.69	1.60	1.41
1.84	1.64	1.25	1.31	1.55	1.24
1.77	1.48	1.08	1.23	1.32	0.53
1.30	1.08	0.48	0.91	0.57	0.17
−0.61	−0.86	−1.10	−1.11	−1.16	−1.39
−2.22	−2.35	−2.43	−2.50	−2.12	−2.44
−2.23	−2.46	−2.70	−2.71	−2.57	−2.73
		Occupied Orbitals			
−5.15	−5.12	−5.15	−5.12	−4.83	−5.32
−5.29	−5.48	−5.50	−5.66	−5.65	−5.92
−6.34	−6.45	−6.39	−6.47	−6.26	−6.45
−6.48	−6.70	−6.91	−6.99	−6.41	−6.71
−7.15	−7.01	−6.98	−7.17	−6.89	−7.09
−7.199	−7.33	−6.98	−7.20	−6.94	−7.16
−7.20	−7.38	−7.67	−7.52	−7.29	−7.42
−7.20	−7.48	−7.71	−7.56	−7.48	−7.48
		Energy Gaps between HOMO and LUMO			
2.92	2.66	2.45	2.41	2.26	2.59
$N_0CPZn(II)$	$N_1CPZn(II)$	*cis*-$N_2CPCu(III)$	*trans*-$N_2CPCu(III)$	$N_3CPZn(IV)$	$N_4CPZn(IV)$
		Virtual Orbitals			
1.87	2.08	1.69	1.87	1.72	
1.87	1.84	1.66	1.52	1.33	1.23
1.36	1.64	1.39	1.31	0.95	1.23
1.19	1.41	1.20	1.07	0.62	0.17
0.86	1.13	−0.80	−0.82	−1.08	−1.41
−0.54	−0.71	−1.85	−1.60	−1.98	−2.52
−2.14	−1.67	−2.01	−2.46	−2.71	−2.53
−2.14	−2.39	−2.42	−2.62	−3.67	−3.79
		Occupied Orbitals			
−5.21	−4.67	−4.88	−4.70	−5.05	−5.99
−5.22	−5.19	−5.33	−5.40	−5.59	−6.62
−6.35	−5.24	−5.83	−5.84	−6.15	−6.69
−6.59	−6.10	−6.54	−6.60	−6.36	−6.94
−6.60	−6.31	−6.72	−6.65	−6.93	−7.34
−6.60	−6.40	−6.77	−6.73	−7.02	−7.38
−7.00	−6.85	−7.23	−7.18	−7.07	−7.67
−7.52	−7.39	−7.74	−7.27	−7.58	−7.81
		Energy Gaps between HOMO and LUMO			
3.07	2.28	2.46	2.08	1.38	1.48

CPCu(III), 1.9272, 1.9264 Å; 1.9825, 1.9902 Å (expt 1.9393, 1.9344 Å; 1.9544, 1.9693 Å[6]), compare to those in *trans*-N_2-CP, 1.9228, 1.9369 Å; 1.9745, 1.9751 Å (expt 1.9407, 1.9447 Å; 1.9656, 1.9676 Å[6]). A little deviation in value is due to the C_6F_5 substitution at meso position in experimental studies.

Electronic structures are fundamental to the interpretation and understanding of the absorption spectra. In Table 2, the calculated frontier orbital energy data (8 occupied orbitals and 8 unoccupied orbitals) are listed, and in Figure 2, molecular orbital energy levels obtained by B3LYP/6-31G* are plotted for comparison. As seen clearly in Figure 2, the energy of the LUMO decreases when the N atom of the pyrrole ring in the core of the porphyrin is inverted to β position to form multiply N-confused porphyrins; however, the energy of the HOMO is little affected with increasing number of confused pyrrole rings except for N_3CP's obvious increase. As a result, the energy gaps of the HOMO and LUMO reduce from N_0CP to multiply N-confused porphyrins (N_0CP 2.92 eV, N_1CP 2.66 eV, *cis*-N_2-CP 2.45 eV, *trans*-N_2CP 2.41 eV, N_3CP 2.26 eV, N_4CP 2.59 eV shown in Table 2). Comparing the frontier orbital energies of a porphyrin and those of its metal complex, as shown in Table 2 and Figure 2, one can find that the HOMO energy of $N_0CPZn(II)$, −5.21 eV, is more stable than that of N_0CP, −5.15 eV, but the LUMOs have an opposite trend, $N_0CPZn(II)$, −2.14 eV, N_0CP, −2.23 eV, thus the energy gaps of HOMO and LUMO increase to 3.07 eV. For N_1CP and N_2CP, their metal complexes' HOMOs and LUMOs all increase, but LUMOs do not increase so much, which leads to a universal reduction of the energy gaps of HOMO and LUMO for $N_1CPZn(II)$, 2.28 eV, *trans*-$N_2CPCu(III)$, 2.08 eV, but almost no change for *cis*-$N_2CPCu(III)$, 2.46 eV. For the N_3CP and N_4CP, there are obvious falls in the energy levels of HOMO and LUMO, especially for $N_4CPZn(IV)$, because the molecules N_3CP and N_4CP change from having no symmetry to possessing C_s symmetry after coordinating to Zn. At the same time, energy gaps of HOMO and LUMO reduce from 2.26 eV, 2.59 eV for N_3CP and N_4CP to 1.38 eV, 1.48 eV for $N_3CPZn(IV)$ and N_4-$CPZn(IV)$.

The standard interpretation of the origin of the Q and B bands in the electronic absorption spectra of porphyrins is based on the four-orbital model of Gouterman,[30] which assumes that the HOMO and HOMO − 1 are almost degenerate in energy and well separated from the other levels; a similar assumption is made for the LUMO and LUMO + 1. Evidently, as can be seen from Figure 2, the four-orbital model approximately describes N_0CP, N_1CP, N_2CP, and $N_0CPZn(II)$ because the other frontier orbitals are separated by a comparatively large energy gap between two highest HOMOs and two lowest LUMOs.

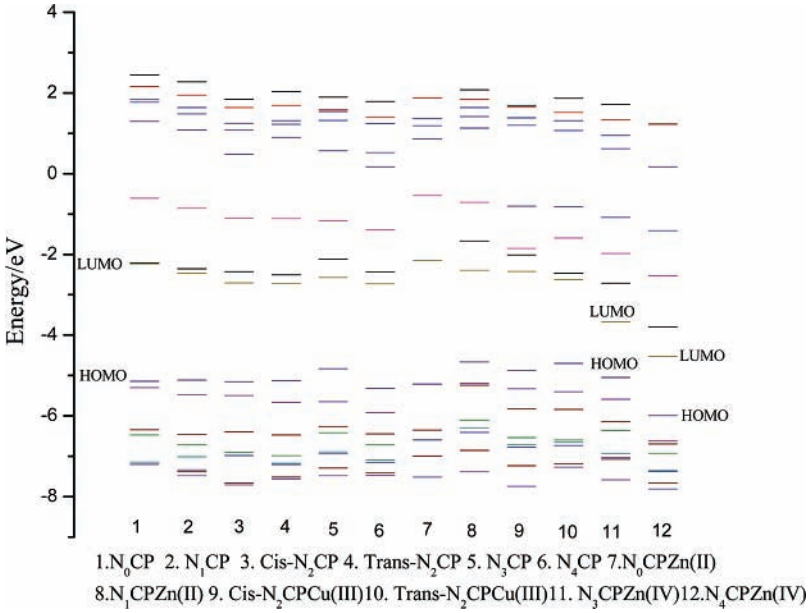

Figure 2. Molecular orbital energy levels.

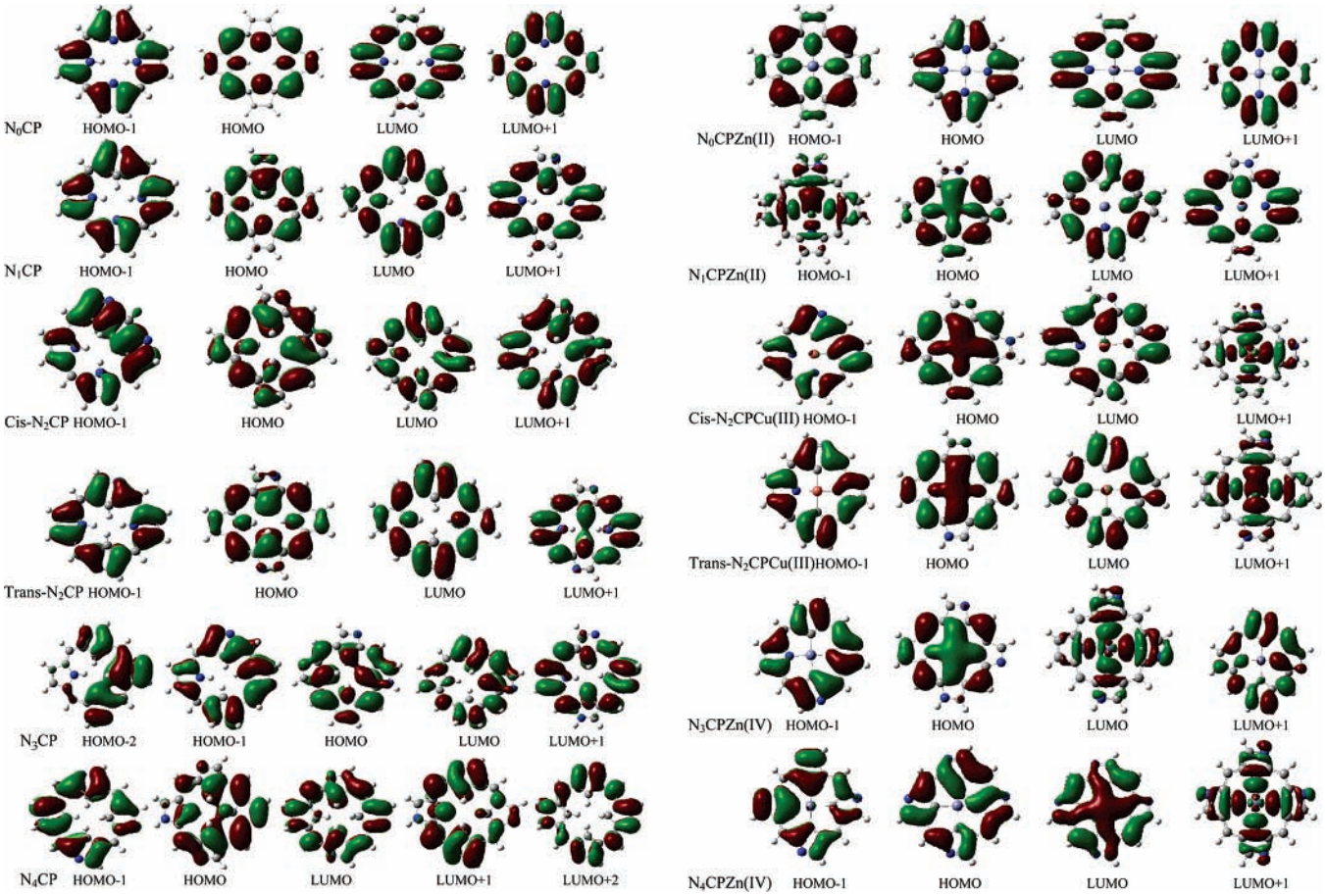

Figure 3. The frontier orbitals of investigated molecules.

However, for other molecules investigated here the four-orbital model is not applicable. So we anticipate that OPA spectra of N_0CPZn(II) will be blue-shifted compared with N_0CP and OPA spectra of *cis*-N_2CP and *trans*-N_2CP are to be red-shifted in comparison with normal porphyrin.

For more intuitional analysis, the shapes of some correlative occupied molecular orbitals and unoccupied molecular orbitals are shown in Figure 3. For normal porphyrin N_0CP, the HOMO $-$ 1 coefficients are localized on $C_\alpha-C_\beta$ of all porphrin rings. HOMO $-$ 1 coefficients are not changed so much except for increasing some coefficients on meso position when the center N atom is inverted to β position. For the HOMO orbital of N_0-CP, the main coefficients are localized on meso and center N atom, in contrast, the basically similar distribution for N_1CP, N_2CP other than some increase coefficients on C_β, but N_3CP, N_4CP change larger than N_1CP, N_2CP so that result in energy

TABLE 3: One-Photon Absorption Properties of All the Molecules

molecule	$\lambda^{(1)}_{max}$ (nm) TDDFT	$\lambda^{(1)}_{max}$ (nm) ZINDO	*f*	transition	$\lambda'^{(1)}_{max}$ (nm) with C_6F_5	exptl data
N_0CP (porphyrin)		618.0	0.01995	$S_0 \rightarrow S_1$		614−626[30,e]
		522.2	0.02431	$S_0 \rightarrow S_2$		512−532[30]
	353.0	358.0	0.83596	$S_0 \rightarrow S_5$	352.9	
	320.7	**345.0**	1.11556	$S_0 \rightarrow S_6$	**342.0**	340[30]
N_0CPZn(II) (ZnP)		552.7	0.04540	$S_0 \rightarrow S_1$,$S_0 \rightarrow S_2$	530.9	558[a],576[b,29]
	349.1	335.0	1.37584	$S_0 \rightarrow S_5$,$S_0 \rightarrow S_6$	326.3	399[a],326[b,29]
N_1CP		662.1	0.00090	$S_0 \rightarrow S_1$	675.5	724[27]
		563.0	0.01191	$S_0 \rightarrow S_2$	563.8	
	402.2	413.1	0.45971	$S_0 \rightarrow S_4$	413.0	438[27,d]
	365.0	**364.0**	1.05363	$S_0 \rightarrow S_6$	**372.6**	
N_1CPZn(II)		629.0	0.04428	$S_0 \rightarrow S_1$		
		547.4	0.12489	$S_0 \rightarrow S_2$		
	386.5	398.5	0.19762	$S_0 \rightarrow S_5$		
	369.9	357.7	0.85518	$S_0 \rightarrow S_7$	366.8	
cis-N_2CP		707.6	0.00904	$S_0 \rightarrow S_1$		
		584.9	0.03206	$S_0 \rightarrow S_2$	600.4	
	460.9	448.6	0.27995	$S_0 \rightarrow S_3$	458.0	
	405.7	**417.9**	0.36464	$S_0 \rightarrow S_5$	**432.9**	424[6,c]
	342.2	328.2	0.33862	$S_0 \rightarrow S_{10}$	333.9	330−340[6]
cis-N_2CPCu(III)	593.8	595.0	0.04281	$S_0 \rightarrow S_2$	604.7	600−610[6]
	418.0	415.9	0.17038	$S_0 \rightarrow S_7$		
	393.7	405.7	0.38501	$S_0 \rightarrow S_8$	400.0	440[6]
	367.7	363.5	0.09880	$S_0 \rightarrow S_9$	370.6	360−370[6]
trans-N_2CP		722.3	0.00893	$S_0 \rightarrow S_1$	743.9	
	558.0	588.9	0.00968	$S_0 \rightarrow S_2$	585.0	
	402.8	397.2	0.66730	$S_0 \rightarrow S_6$	398.0	449[6]
	385.0	**376.5**	1.07340	$S_0 \rightarrow S_7$	**382.7**	350−360[6]
trans-N_2CPCu(III)	735.9	744.0	0.09722	$S_0 \rightarrow S_2$	764.0	
		541.2	0.06660	$S_0 \rightarrow S_4$	555.3	580[6]
	508.2	490.6	0.01423	$S_0 \rightarrow S_5$		490−495[6]
	438.4	417.3	0.31673	$S_0 \rightarrow S_7$	421.3	440[6]
	343.7	366.8	0.28865	$S_0 \rightarrow S_{11}$	372.0	337[6]
N_3CP	548.0	562.0	0.04423	$S_0 \rightarrow S_1$	580.0	
	424.0	435.9	0.03115	$S_0 \rightarrow S_3$	430.4	
	375.0	370.2	0.52848	$S_0 \rightarrow S_4$	388.2	
	368.8	**360.7**	0.53035	$S_0 \rightarrow S_5$	**374.7**	
N_3CPZn(IV)		600.8	0.06027	$S_0 \rightarrow S_5$	618.8	
		526.3	0.03038	$S_0 \rightarrow S_6$	528.2	
	513.3	517.0	0.03203	$S_0 \rightarrow S_7$		
	410.1	407.0	0.17135	$S_0 \rightarrow S_{13}$	411.8	
	385.6	388.8	0.20409	$S_0 \rightarrow S_{14}$	392.6	
N_4CP	523.0	531.6	0.01808	$S_0 \rightarrow S_1$	548.3	
	399.9	**378.8**	0.64115	$S_0 \rightarrow S_4$	**390.7**	
	338.1	352.2	0.50108	$S_0 \rightarrow S_5$	363.1	
N_4CPZn(IV)	561.8	558.3	0.02448	$S_0 \rightarrow S_6$	541.3	
		531.3	0.02341	$S_0 \rightarrow S_8$	520.0	
	400.3	401.3	0.07102	$S_0 \rightarrow S_{11}$	388.3	
		329.5	0.07627	$S_0 \rightarrow S_{20}$	319.6	

[a] Experimental value of the ZnP with four C_6F_5- substituents in ref 29. [b] Calculated value of ZnP with four C_6F_5- substituents in ref 29. [c] The experimental value in ref 6 is the absorption spectra value of corresponding N-confused porphyrins with four C_6F_5- substituents at meso position. [d] The experimental value in ref 27 is the absorption spectra value of single N-confused tetraphenyl porphyrin. [e] Experimental value of normal porphyrin without any substituent in ref 30.

change vitally. For LUMO and LUMO + 1 of N_0CP, the main coefficients are both localized on meso and two $C_\alpha-C_\beta$ in spite of different orientation of $C_\alpha-C_\beta$. And the multiply N-confused porphyrins have similar distribution except that LUMO and LUMO + 1 of N_1CP, N_2CP, and N_3CP have opposite orientation of $C_\alpha-C_\beta$ compared with N_0CP. There is intermolecular charge transfer to some extent for multiply N-confused porphyrins, which is deemed to be effective in enhancing the two-photon absorptivity irrespective of the direction of the transfer. As seen in Figure 3, when metals coordinate to multiply N-confused porphyrins, the coefficients on HOMOs of metal complexes are almost similar, and are enhanced on the metal center compared with corresponding multiply N-confused porphyrins. But the N_4CP is an exception. So its energy of HOMO occur large decrease, the same result for LUMO.

2. One-Photon Absorption. One-photon absorption properties of all the investigated molecules are calculated by using the ZINDO program on the basis of optimized geometric structures. The active Q and Soret bands with large OPA intensities and the corresponding oscillator strength and transition nature are listed in Table 3, and some experimental data are given. At the same time for proving the veracity of the ZINDO method for calculating spectra, the TDDFT method is also adopted to calculate the one-photon absorption spectra. Comparing these two results by TDDFT and ZINDO as shown in Table 3, we can find that the differences beween them are very little (average15 nm). Therefore, a semiempirical ZINDO method is appropriate for these selected molecules in this work, and sometimes the results by the ZINDO method are closer to the experimental data. Table 3 indicates that the value of N_0CP

calculated by ZINDO is in better agreement with the experimental observations because the experimental observations achieved for the gas-phase absorption spectrum are the same as the conditions of our calculation. However, calculated OPA spectra values of other molecules with experimental data are generally smaller than the experimental observation values. This is because experimental measurement was done with the corresponding molecules with substituents at meso position in CH_2Cl_2 solvent, and the substituents at meso position usually make the spectra shift. For seeing about the influence of the substituents at meso position, one-photon absorption spectra of corresponding molecules with C_6F_5 substituents are also calculated. As shown in Table 3, the results show a good coherence with experiment results, and differences (1−21 nm) between molecules without any substituent and those with C_6F_5 substituents are not large. It is believed that there is no effect to comparison study of normal porphyrin and multiply N-confused porphyrins. Therefore later discussion is based on the results of molecules without any substituent by the ZINDO method.

As shown in Table 3, the Soret peak with the largest oscillator strength is red-shifted when the N atom in the normal porphyrin core is inverted to β position (N_0CP 345 nm; N_1CP 364 nm; *cis*-N_2CP 417.9 nm; *trans*-N_2CP 376.5 nm; N_3CP 360.7 nm; N_4CP 378.8 nm shown in boldface in Table 3), and the same rule for Q-band absorption of N_1CP, *cis*-N_2CP, *trans*-N_2CP. Q-band absorption is generally contributed by HOMO and LUMO orbitals according to the four-orbital model; therefore, as shown in Figure 2 and Table 2, decreasing the energy gap between HOMO and LUMO result in the red-shift. Examining the influence of metal coordination, one can find that the Soret peak of normal porphyrin Zn complex is a little blue-shifted, 10 nm, relative to porphyrin because the energy gap between HOMO and LUMO increased from 2.92 eV to 3.07 eV, and the same blue-shifted trend is observed for N_1CP, N_2CP, and N_4CP's metal complexes, and only $N_3CPZn(IV)$ is red-shifted about 28 nm. The results in Table 3 also demonstrate that the OPA intensities of the multiply N-confused porphyrin molecules are decreased with the inverted N atoms one by one from core to β position. The structural change on the macrocycle leads to a decrease in symmetry and a reduction in aromaticity (conjugation) as compared to normal porphyrin, as well as photophysical properties.

3. Two-Photon Absorption. It is well-known that one- and two-photon absorptions adhere to different selection rules. For the molecule that has central symmetry, a change in the parity between the initial and final states (wave functions) is required for every photon involved in the transition for electric dipole transitions. Thus the selection rule for TPA is different from that of OPA. One change of parity is required for a one-photon transition, while two-photon transitions must have initial and final states with the same parity. For our investigated molecules: N_0CP (porphyrin), N_0CPZn (ZnP), and *trans*-N_2CP have center symmetry, others have no center symmetry. According to the rules above, for every molecule, we selected several excited states that two-photon absorption allowed as the two-photon absorption final states and calculated the two-photon absorption cross sections δ, and then we obtained the maximum δ_{max} and corresponding λ_{max} for every molecule. In order to provide more clear comparison for studied molecules in this work, two-photon absorption spectra in the incident wavelength range of 500−1200 nm are shown in Figure 4 and Figure 5. The calculated TPA maximum absorption wavelength λ_{max}, transition nature, configurations and weights, and maximum TPA cross section δ_{max} of all molecules are summarized in Table 4.

a. Effects of Substituents. For examing the effects of substituents, TPA cross sections of tetraphenyl-porphyrin ($4C_6H_5-N_0CP$) and all corresponding molecules with $-C_6F_5$s at meso-position were also calculated with ZINDO/SOS as shown in Table 4. The calculated result of tetraphenyl-porphyrin (TPA maximum absorption wavelength λ_{max}, 647 nm; TPA cross section δ_{max}, 99.4 GM) is on the whole consistent with the experimental result (647 nm and 15 GM).[32] The calculated and experimental values of the TPA cross section δ_{max} are somewhat different owing to the different experimental conditions (such as solvent effect) and excited wavelength used by the experimental study, but two results have the same magnitude. For ease of comparison, two-photon absorption spectra of N_0CP, $4C_6H_5-N_0CP$, and $4C_6F_5-N_0CP$ are plotted in Figure 5. We can clearly find in Figure 5 that the order of the TPA cross section δ_{max} is $N_0CP < 4C_6H_5-N_0CP < 4C_6F_5-N_0CP$ (52.58 < 99.4 < 134.6 GM) and the order of TPA λ_{max} is opposite (658.8 > 647 > 559.2 nm). Therefore, the electron donors at meso-position make the TPA cross section δ_{max} increase, and the stronger the electron donors are, the more the TPA cross section δ_{max} increases. It is also the same with multiply N-confused porphyrins and their Cu or Zn complexes and the corresponding TPA cross section δ_{max} of those with $-C_6F_5$ substituents are shown in Table 4 in comparison with those without any substituent.

b. Comparison of Multiply N-Confused Porphyrins and Normal Porphyrin. For ease to lengthwise comparison of multiply N-confused porphyrins and normal porphyrin, the substituents are not involved in later discussion. As shown in Table 4, the TPA maximum absorption wavelength λ_{max} of normal porphyrin is 658.8 nm; the TPA cross section δ_{max} is 52.58 GM. It is observed that the maximum absorption wavelengths λ_{max} are blue-shifted and the TPA cross sections δ_{max} are increased 22.7−112.1 GM when N atoms one by one are inverted from core to β position to form multiply N-confused porphyrins (shown in boldface in Table 4). From the surface point of view, the decrease in symmetry and aromaticity (or conjugation) for multiply N-confused porphyrins as compared to normal porphyrin would make them more weak on the photophysical properties. However, the interpretation for two-photon absorption by using the conjugation theory is not complete. A three-level energy model can give a rough explanation. Generally, the position and relative strength of the two-photon response are to be predicted using the following simplified form of the SOS expression,[31]

$$\delta \propto \frac{M_{0k}{}^2 M_{kn}{}^2}{(E_{0k} - E_{0n}/2)^2 \Gamma} + \frac{M_{0n}{}^2 \Delta\mu_{0n}{}^2}{(E_{0n}/2)^2 \Gamma} \qquad (4)$$

where M_{ij} is the transition dipole moment from state i to j; E_{ij} is the corresponding excitation energy; the subscripts 0, k, and n refer to the ground state S_0, the intermediate state S_k, and the TPA final state S_n, respectively; and $\Delta\mu_{0n}$ is the dipole moment difference between S_0 and S_n, which is zero in centrosymmetric molecules. So for centrosymmetric molecules, eq 4 becomes the following formula:

$$\delta \propto \frac{M_{0k}{}^2 M_{kn}{}^2}{(E_{0k} - E_{0n}/2)^2 \Gamma} \qquad (5)$$

For molecules N_0CP, N_1CP, *cis*-N_2CP, *trans*N_2CP, N_3CP, and

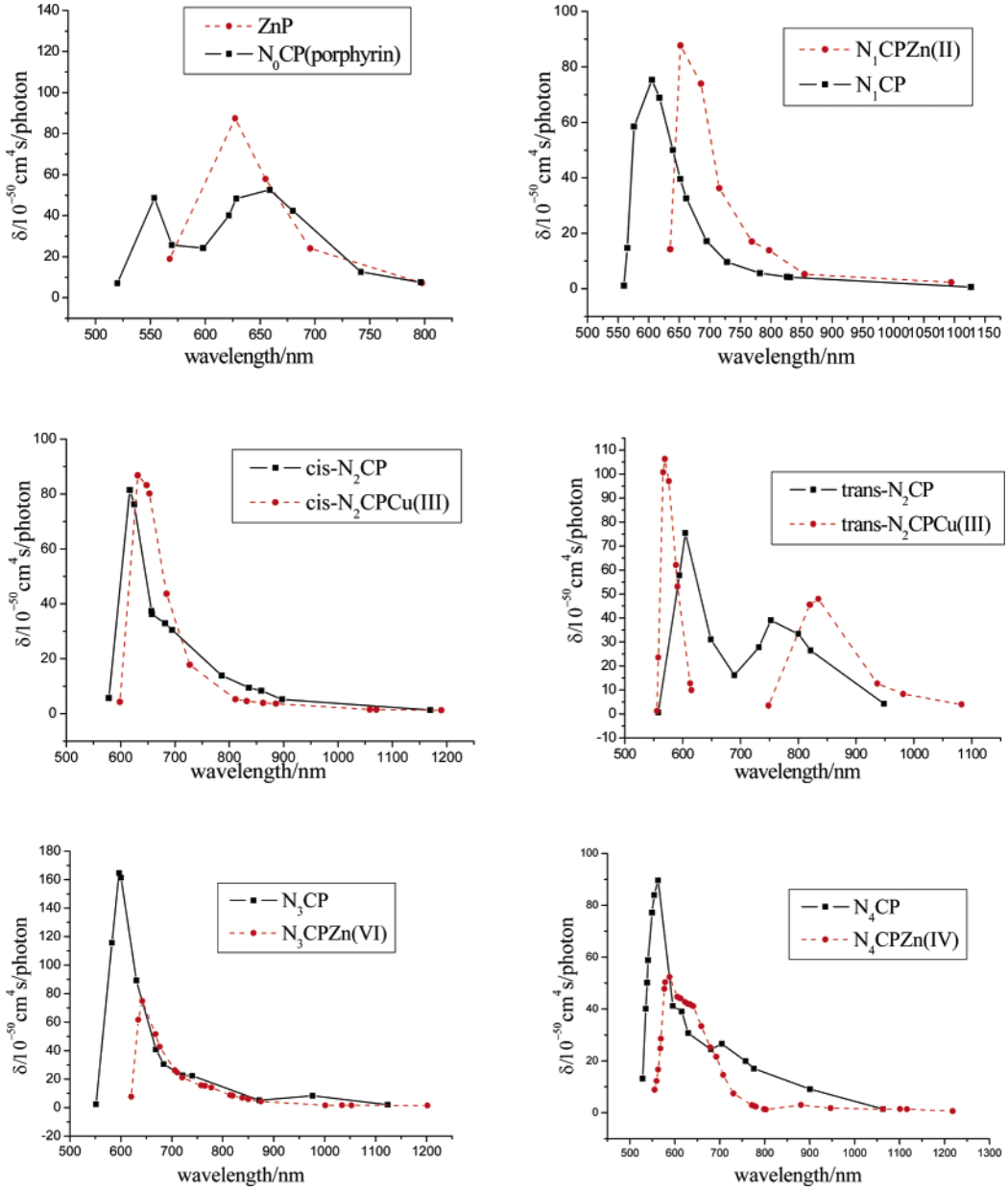

Figure 4. Two-photon absorption spectra.

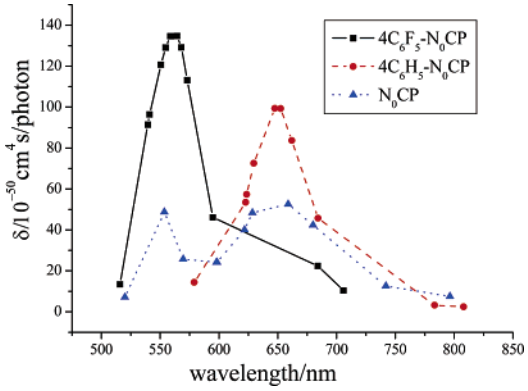

Figure 5. Two-photon absorption spectra comparison of N_0CP, $4C_6H_5-N_0CP$, and $4C_6F_5-N_0CP$.

N_4CP, data and parameters needed in three-level energy equation 4 and calculated results of eq 4 are listed in Table 5. It is clear that results of eq 4 have the same increasing trend with the δ_{max} when comparing N-confused porphyrins and normal porphyrin. As shown in Table 5, for N_1CP, *trans*N_2CP, and N_4-CP, the visible increase of the transition dipole moment M_{0k} takes main responsibility for increasing the maximum TPA cross section δ_{max} compared to N_0CP. However, for *cis*-N_2CP and N_3CP, the difference between E_{0k}, the transition energy from S_0 to S_k, and $E_{0n}/2$, half of the transition energy from S_0 to S_n, is the main reason.

c. Effects of Metal Coordination. Now we pay attention to the effect of Zn or Cu coordination. One can observed from Figure 4 that the TPA cross section δ_{max} values are enhanced when metals are coordinated to porphyrin and singly and doubly N-confused porphyrins probably due to the enhanced planar conjugation. However, the observation for N_3CP and N_4CP is the reverse. As seen in Table 5, the transition dipole moment of N_3CP is not very large but the difference between transition energies $E_{0k} - E_{0n}/2$ is very small. Furthermore, the main configuration of N_3CP, as seen in Table 4, is HOMO − 2, 0 → LUMO, 0. It is worth noting that a more obvious intermolecular

TABLE 4: TPA Properties of All the Selected Molecules in This Paper

molecules	$\lambda^{(2)}_{max}$ (nm)	transition	configurations and weights	δ_{max} (GM)[a]	δ'_{max} with $4C_6F_5$
N_0CP (porphyrin)	**658.8**	$S_0 \rightarrow S_8$	(HOMO, 0) → (LUMO + 3, 0) 14%	**52.58**	134.6
$4C_6H_5-N_0CP$	647(647)		(HOMO, HOMO) → (LUMO, LUMO + 1) 31%	99.4(15)[32,b]	
$N_0CPZn(II)$ (ZnP)	627.2	$S_0 \rightarrow S_8$	(HOMO, 0) → (LUMO + 3, 0) 22%	**87.44**	**92.4**
			(HOMO, HOMO) → (LUMO, LUMO) 26%		
			(HOMO, HOMO) → (LUMO + 1, LUMO + 1) 26%		
N_1CP	**605.2**	$S_0 \rightarrow S_{12}$	(HOMO, 0) → (LUMO + 3, 0) 16%	75.28	165
			(HOMO, HOMO) → (LUMO + 1, LUMO + 1) 19%		
$N_1CPZn(II)$	652	$S_0 \rightarrow S_9$	(HOMO − 2, 0) → (LUMO + 1, 0) 90%	87.71	207
cis-N_2CP	**616.8**	$S_0 \rightarrow S_{12}$	(HOMO − 1, HOMO − 1) → (LUMO, LUMO + 1) 14%	**81.44**	**125**
			(HOMO − 1, HOMO) → (LUMO + 1, LUMO + 1) 24%		
			(HOMO, HOMO) → (LUMO, LUMO + 1) 30%		
cis-$N_2CPCu(III)$	631.4	$S_0 \rightarrow S_{13}$	(HOMO − 1, HOMO) → (LUMO, LUMO + 2) 21%	86.78	120
			(HOMO, HOMO) → (LUMO, LUMO + 2) 53%		
trans-N_2CP	752.6	$S_0 \rightarrow S_{12}$	(HOMO − 1, 0) → (LUMO, 0) 46%	39.05	121
			(HOMO, 0) → (LUMO + 1, 0) 31%		
	604.6	$S_0 \rightarrow S_8$	(HOMO − 1, HOMO − 1) → (LUMO, LUMO) 19%	**75.5**	**223**
			(HOMO − 1, HOMO) → (LUMO, LUMO + 1) 32%		
			(HOMO, HOMO) → (LUMO + 1, LUMO + 1) 15%		
trans-$N_2CPCu(III)$	834.6	$S_0 \rightarrow S_7$	(HOMO − 2, 0) → (LUMO + 1, 0) 51%	47.98	
			(HOMO − 1, 0) → (LUMO + 1, 0) 15%		
			(HOMO − 1, HOMO) → (LUMO, LUMO + 1) 16%		
	569.4	$S_0 \rightarrow S_{21}$	(HOMO − 2, HOMO) → (LUMO, LUMO + 1) 40%	106.3	265
N_3CP	**596.6**	$S_0 \rightarrow S_{10}$	(HOMO − 2, 0) → (LUMO, 0) 25%	**164.7**	**565**
			(HOMO − 1, 0) → (LUMO + 2, 0) 20%		
$N_3CPZn(IV)$	642	$S_0 \rightarrow S_{22}$	(HOMO − 4, 0) → (LUMO, 0) 18%	74.8	445
			(HOMO − 1, HOMO) → (LUMO, LUMO + 1) 20%		
N_4CP	704.4	$S_0 \rightarrow S_5$	(HOMO − 1, 0) → (LUMO, 0) 50%	26.6	
			(HOMO, 0) → (LUMO + 1, 0) 16%		
	563	$S_0 \rightarrow S_{10}$	(HOMO − 3, 0) → (LUMO, 0) 15%	**89.6**	**365**
			(HOMO − 1, 0) → (LUMO + 2, 0) 35%		
$N_4CPZn(IV)$	641	$S_0 \rightarrow S_{21}$	(HOMO − 2, 0) → (LUMO + 3, 0) 20%	41.1	44.3
			(HOMO − 1, 0) → (LUMO + 3, 0) 13%		
	588.6	$S_0 \rightarrow S_{29}$	(HOMO − 2, 0) → (LUMO + 2, 0) 17%	52.4	

[a] 1 GM = 10^{-50} cm^4 s/photon. [b] The value in the brace is the TPA experimental datum of tetraphenyl-porphyrin in toluene in ref 32.

TABLE 5: Data and Parameters of Three-Level Energy Model for Multiply N-Confused Porphyrins

	M_{0k}^2	M_{kn}^2	M_{0n}^2	$\Delta\mu_{0n}^2$	E_{0k} (eV)	E_{0n} (eV)	Γ	X[a]	δ_{max} (GM)
N_0CP	2.695	2.024	0	0	2.37	3.76	0.14	162.2714	52.58
N_1CP	81.44	5.08	0.34	0.0424	3.40	4.10	0.14	1621.483	75.28
cis-N_2CP	3.98	1.926	0.175	13.98	2.12	4.02	0.14	4529.402	81.44
trans-N_2CP	85.82	6.75	0	0	3.29	4.10	0.14	2691.044	75.5
N_3CP	5.279	2.457	4.27	0.831	2.21	4.15	0.14	5089.368	164.7
N_4CP	50.68	10.47	37.48	6.03	3.27	3.52	0.14	2183.42	89.6

[a] $X = (M_{0k}^2 M_{kn}^2)/[(E_{0k} - E_{0n}/2)^2\Gamma] + (M_{0n}^2\Delta\mu_{0n}^2)/[(E_{0n}/2)^2\Gamma]$.

charge transfer from HOMO − 2 to LUMO of N_3CP is found in Figure 3, which is very beneficial to interpret the increase of the TPA cross section. Therefore, N_3CP exhibits the largest TPA cross section, 164 GM (three times that of N_0CP), in the middle of all investigated N-confused molecules in this work, and the δ_{max} of its Zn complex does not exceed that of N_3CP although the planar conjugation is enhanced. Similarly, the main configuration of N_4CP is HOMO − 1, 0 → LUMO + 2, 0 (35%), and there is more obvious intermolecular charge transfer in N_4-CP than that in its Zn complex $N_4CPZn(IV)$ as seen in Figure 3.

In addition, for *trans*N_2CP, N_4CP, and their metal complexes, there is another TPA peak at a longer wavelength (752.6 nm, 834.6 nm, 704.4 nm, and 641 nm) as shown in Figure 4. We also list these TPA δ_{max} and corresponding wavelength in Table 4 to provide some useful information for experimental applied studies, because the TPA responding wavelength is located in the IR or near-IR region, which is important to exploit the field of photodynamic therapy, in spite of lower two-photon absorption cross section than normal porphyrin. In particular, Cu(III) complexes of *cis*- and *trans*-N_2CP have the peripheral NH and N, which behave as hydrogen bonding donor and acceptor. In the solid state both complexes can form supramolecular networks, which have been synthesized by Maeda groups.[5,6] It is expected that this kind of supramolecular network would behave excellent photophysical properties. Therefore it is believed that our investigation on the multiply N-confused porphyrins will be useful for deeper study on the photophysical properties of new materials made of multiply N-confused porphyrins.

Conclusions

Systemic theoretical investigations of the electronic structure, one-photon absorption (OPA), and TPA properties have been completed, and the structure−property relationship has been revealed. Our studied results indicate that the OPA spectra of multiply N-confused porphyrins are red-shifted and the OPA intensities are decreased compared to normal porphyrin. At the same time, the maximum two-photon absorption wavelengths λ_{max} are blue-shifted and the TPA cross sections δ_{max} are increased 22.7−112.1 GM when N atoms one by one are

inverted from core to β position to form multiply N-confused porphyrins. Especially the δ_{max} of N_3CP reaches 164.7 GM because of the small difference between transition energies $E_{0k} - E_{0n}/2$ and a more obvious intermolecular charge transfer from HOMO − 2 to LUMO. The electron donors at meso-position make the TPA cross section δ_{max} increase, and the stronger the electron donors are, the more the TPA cross section δ_{max} increases. δ_{max} of N_3CP with four C_6F_5s reaches 565 GM. After forming metal complexes with Cu or Zn, the TPA properties of multiply N-confused porphyrins are further increased except for N_3CP, N_4CP. So we believe that this will provide some useful information for designing and synthesizing materials with large TPA cross sections. In addition, for *trans*N_2CP, N_4CP, and their metal complexes, there is another TPA peak at longer IR or near-IR wave region. Although the corresponding TPA cross section is smaller than that of normal porphyrin, people can exploit their application in the field of photodynamic therapy by assembling materials such as supramolecular networks of *cis*- and *trans*-N_2CP.

Acknowledgment. This work is supported by the National Nature Science Foundation of China and the Key Laboratory for Supramolecular Structure and Material of Jilin University.

References and Notes

(1) Shelnutt, J. A.; Song, X. Z.; Ma, J. G.; Jia, S. L.; Jentzen, W.; Medforth, C. *J. Chem. Soc. Rev.* **1998**, *27*, 31−41.

(2) Ishizuka, T.; Osuka, A.; Furuta, H. *Angew. Chem., Int. Ed.* **2004**, *43*, 5077−5081.

(3) Furuta, H.; Asano, T.; ogawa, T. *J. Am. Chem. Soc.* **1994**, *116*, 767−768.

(4) Chmielewski, P. J.; Latos-Grażyński, L.; Rachlewicz, K.; Głowiak, T. *Angew. Chem., Int. Ed. Engl.* **1994**, *33*, 779−781.

(5) Furuta, H.; Maeda, H.; Osuka, A. *J. Am. Chem. Soc.* **2000**, *122*, 803−807.

(6) Maeda, H.; Osuka, A.; Furuta, H. J. *Am. Chem. Soc.* **2003**, *125*, 15690−15691.

(7) Furuta, H.; Maeda, H.; Osuka, A. *J. Am. Chem. Soc.* **2001**, *123*, *6435*.

(8) Furuta, H.; Maeda, H.; Osuka, A. *Chem. Commun.* **2002**, 1795−1804.

(9) Maeda, H.; Ishikawa, Y.; Matsuda, T.; Osuka, A.; Furuta, H. *J. Am. Chem. Soc.* **2003**, *125*, 11822−11823.

(10) Srinivasan, A.; Furuta, H. *Acc. Chem. Res.* **2005**, *38*, 10.

(11) Chen, P.; Tomov, I. V.; Dvovnikov, A. S.; Nakashima, M.; Roach, J. F.; Alabram, D. M.; Rentzepis, P. M. *J. Phys. Chem.* **1996**, *100*, 17507.

(12) Karotki, A.; Drobizhev, M.; Kruk, M.; Spangler, C.; Nickel, E.; Mamardashvili, N.; Rebane, A. *J. Opt. Soc. Am. B* **2003**, *20*, 321.

(13) Yamashita, M.; Tamono, T.; Kobayashi, S.; Torizuka, K.; Aizawa, K.; Sato, T. *Photochem. Photobiol.* **1988**, *47*, 189.

(14) Meshalkin Yu, P.; Alfimov, E. E.; Vasil'ev, N. E.; Denisov, A. N.; Makukha, V. K.; Ogirenko, A. P. *Quantum. Electron*. **1999**, *29*, 1066.

(15) Goyan, R. L.; Gramb, D. T. *Photochem. Photobiol.* **2000**, *72*, 821.

(16) Ogawa, K.; Zhang, T.; Yoshihara, K.; Kobuke, Y. *J. Am. Chem. Soc.* **2002**, *124*, 22.

(17) Ogawa, K.; Ohashi, A.; Kobuke, Y.; Kamada, K.; Ohta, K. *J. Am. Chem. Soc.* **2003**, *125*, 13356.

(18) Zhou, X.; Ren, A. M.; Feng, J. K.; Liu, X. J. *Chem.—Eur. J.* **2004**, *10*, 5623.

(19) Zhou, X.; Ren, A. M.; Feng, J. K.; Shuai, Z. G. *J. Photochem. Photobiol. A: Chem.* **2005**, *172*, 126.

(20) Cha, M.; Torruellas, W. E.; Stegeman, G. I.; Horsthuis, W. H. G.; Möhlmann, G. R. *J. Methods Appl. Phys. Lett.* **1994**, *65*, 2648.

(21) Kogej, T.; Beljonne, D.; Meyers, F.; Perry, J. W.; Marder, S. R.; Brédas′, J.-L. *Chem. Phys. Lett.* **1998**, *298*, 1.

(22) Orr, B. J.; Ward, J. F. *Mol. Phys.* **1971**, *20*, 513.

(23) Bishop, D. M.; Luis, J. M.; Kirtman, B. *J. Chem. Phys.* **2002**, *116*, 9729.

(24) Albota, M.; Beljonne, D.; Brédas′, J. L.; Ehrlich, J. E.; Fu, J.; Heikal, A. A.; Hess, E.; Kogej, T.; Levin, M. D.; Marder, S. R.; McCord-Maughon, D.; Perry, W.; RÖeckel, H.; Rumi, M.; Subramaniam, G.; Webb, W. W.; Wu, X.; Xu, C. *Science* **1998**, *281*, 1653.

(25) Morel, Y.; Irimia, A.; Najechalski, P.; Kervella, Y.; Stephan, O.; Baldeck, P. L.; Andraud, C. *J. Chem. Phys.* **2001**,*114*, 5391.

(26) Furuta, H.; Maeda, H.; Osuka, A. *J. Org. Chem.* **2001**, *66*, 8563−8572.

(27) Furuta, H.; Ishizuka, T.; Osuka, A.; Dejima, H.; Nakagawa, H.; Ishikawa, Y. *J. Am. Chem. Soc.* **2001**, *123*, 6207−6208.

(28) Edwards, L.; Dolphin, D. H.; Gouterman, M.; Adler, A. D. *J. Mol. Spectrosc.* **1971**, *38*, 16.

(29) LeCours, S. M.; DiMagno, S. G.; Therien, M. J. *J. Am. Chem. Soc.* **1996**, *118*, 11854−11864.

(30) Gouterman, M. *J. Chem. Phys.* **1960**, *33*, 1523.

(31) Rumi, M.; Ehrlich, J. E.; Heikal, A. A.; Perry, J. W.; Barlow, S.; Hu, Z.; McCord-Maughon, D.; Parker, T. C.; Röckel, H.; Thayumanavan, S.; Marder, S. R.; Beljonne, D.; Brédas, J. L. *J. Am. Chem. Soc.* **2000**, *122*, 9500.

(32) Drobizhev, M.; Karotki, A.; Kruk, M.; Rebane, A. *Chem. Phys. Lett.* **2002**, *355*, 175.